

Accelerated vibration-fatigue characterization for 3D-printed structures: Application to fused-filament-fabricated PLA samples

Martin Česnik^{a,*}, Janko Slavič^a, Miha Boltežar^a

^a*University of Ljubljana, Faculty of Mechanical Engineering, Aškerčeva 6, 1000
Ljubljana, Slovenia*

Cite as:

*M. Česnik, J. Slavič and M. Boltežar,
Accelerated vibration-fatigue characterization for 3D-printed structures:
Application to fused-filament-fabricated PLA samples,
International Journal of Fatigue, Vol. 171(2023), 107574,
DOI: 10.1016/j.ijfatigue.2023.107574*

Abstract

Numerous processing parameters combined with long-duration fatigue tests pose a major challenge when assessing the fatigue parameters of 3D-printed structures. In this research, a fatigue-testing method is introduced where sample is excited with random-signal profile enclosing sample's natural frequency. The innovative sample design is tailored for 3D-printing and is frequency-tuneable. The proposed approach results in significantly shorter fatigue tests due to higher loading frequency and simultaneous testing of multiple samples. Additionally, tracking of sample's natural frequency and damping during fatigue tests is applicable. The proposed method was experimentally verified on PLA samples; obtained results were comparable with the available literature.

Keywords:

- Accelerated fatigue test

*Corresponding author. Tel.: +386 14771 227.
Email address: martin.cesnik@fs.uni-lj.si

- Random-signal excitation
 - Specimen design
 - Fused filament fabrication
-

1. Introduction

Fused Filament Fabrication (FFF) is the most widely used [1] additive-manufacturing (AM) technology. Although limited to thermoplastic materials, FFF has gained significant attention from the scientific community for a wide range of applications, from single-process-printed accelerometers [2] and embedded wires [3] and sensors [4] to various types of metamaterials [5]. Considering the advantages of AM and the possible use of biodegradable materials such as polylactic acid (PLA), FFF represents a promising alternative to conventional injection-molding technology for the production of functional components and systems. To ensure the reliability of the components manufactured with FFF and subjected to dynamic loads during their service life, a comprehensive characterization of their mechanical properties is necessary.

The mechanical properties of components produced with FFF are highly dependent on the processing parameters (*e. g.* printer-bed and nozzle temperature, nozzle diameter, layer height, infill pattern and density, feed rate, number of perimeter layers, etc.); Khosravani et al. [6], for example, studied the influence of printing speed and raster angle on the mechanical properties of PLA parts under a static load. In addition, thermoplastic materials used for FFF show a strong dependence on loading (strain rate, loading frequency, etc.) and environmental conditions (temperature, humidity, ageing), as studied by Luo et al. [7]. Clearly, extensive experimental studies are required for a thorough characterization of FFF components.

Although most studies of FFF components deal with static tensile and flexural tests, recently there has been an increased interest in the fatigue properties of FFF components, see Rouf et al. [8]. One of the first studies of the fatigue of FFF components was performed by Afrose et al. [9], followed by studies by Jerez-Mesa et al. [10] and Gomes-Gras et al. [11], which investigated the fatigue life of FFF PLA in the low-cycle regime. A comprehensive study at the high-cycle fatigue limit was conducted by Ezech et al. [12], in which the influence of load ratio and raster orientation on the fatigue properties of FFF PLA components were investigated, followed by another study by

Ezeh et al. [13], focusing on the presence of a notch. Mayén et al. [14] studied the effect of raster angle and heat treatment on the fatigue life and hardness of FFF PLA samples with a cylindrical geometry. Interest in the fatigue of FFF components is not limited to PLA; recent studies on the fatigue of 3D-printed ABS by He et al. [15] and Ziemian et al. [16], wood-induced PLA by Travieso-Rodrigues et al. [17], plain PA6 by Terekhinna et al. [18], carbon-fiber-reinforced PA6 by Li et al. [19], biodegradable polymer materials (PBS and PBAT) by Zhang et al. [20] and friction-stir-welded joints between PLA and ABS by Parast et al. [21] were published. Shanmugam et al. [22] and Crawford and Martin [23] report that accelerating fatigue tests by increasing the loading frequency can potentially lead to ductile fatigue failure and a significantly shorter fatigue life. Consequently, low loading frequencies are required, resulting in long test times, which, in combination with a variety of processing, loading, and environmental parameters, are the main bottleneck in the fatigue characterization of FFF components.

When the loading frequency exceeds the quasi-static range and coincides with the frequency range of the component's natural frequencies, failure due to vibration fatigue [24] can occur. This depends on the modal properties of the component (natural frequencies, mode shapes, and damping) and the type of loading. The dynamic response of FFF components recently attracted the attention of researchers: Xue et al. [25] investigated the influence of processing parameters on the natural frequency and damping ratio of a FFF PLA component, Medel et al. [26] observed good repeatability of sample's natural frequencies and a large scatter of the damping ratios for a given set of processing parameters. In the study by Palmieri et al. [27], the fatigue failure of a FFF PLA component was achieved under vibration loading, and excellent agreement was found between the actual fatigue lives at a loading frequency of approx. 200 Hz, and the estimated fatigue lives, obtained from fatigue tests at a frequency of 4 Hz. Although the extrapolation of the loading frequency did not appear critical in [27], the strong dependence of the polymer's mechanical characteristics on the strain rate indicates the need for a thorough investigation of the fatigue parameters of a FFF component as a function of the loading frequency and strain rate.

This manuscript presents a novel approach to determining the fatigue properties of FFF components by exciting the sample with a broadband random signal in the frequency range of the sample's natural frequency using an electrodynamic shaker. The improvements of this approach over classical fatigue testing are: the fatigue testing times are much shorter, the novel

70 sample design offers the possibility of frequency tuning and thus the explo-
ration of frequency-dependent fatigue parameters. In addition, the proposed
methodology allows the initial natural frequencies and damping ratios of the
FFF samples, as well as their changes during damage accumulation, to be
determined and later used to create a digital twin of the component or for
75 fatigue monitoring.

This manuscript is organized as follows. First, the theoretical background
of relevant topics in the fields of structural dynamics and spectral methods for
damage estimation is given in Sec. 2. Sec. 3 introduces the vibration-fatigue-
based testing methodology from the experimental and modeling aspect. Dif-
80 ferent sets of test samples used for affirmation of the new methodology are
presented in Sec. 4. An evaluation of all the experimental data is presented in
Sec. 5, where fatigue parameters of tested sample sets are extracted and com-
pared reciprocally, and with data from the available literature. Conclusions
are drawn in Sec. 6.

85 2. Theoretical background

The basic concept of accelerated fatigue testing in this research follows
the vibration-testing approach using an electrodynamic shaker [28]. An elec-
trodynamic shaker utilizes the required kinematics (commonly within the
frequency range 5-2000Hz) at the shaker armature (Fig. 1). The test sample
90 is fixed to the shaker armature; while the fixation has to be carefully designed
to provide rigid fixation conditions, the sample is regarded as a flexible dy-
namic system, see Fig. 1. This section addresses the necessary theoretical
aspects, relevant to understanding the relationship between the base kine-
matics and the damage accumulation with a consequent fatigue failure of
95 the sample [24]. Arising from the known kinematics of the shaker armature,
Sec. 2.1 presents the theory for obtaining the stress response in the sample's
fatigue zone. Once the sample's stress response is known, the spectral meth-
ods summarized in Sec. 2.2, provide an estimation of the sample's fatigue
life. For more theoretical details on Secs. 2.1 and 2.2, the interested reader
100 is referred to [28, 29] and [24, 30], respectively.

2.1. Stress response under a base excitation vibration load

The absolute position of a dynamic system with N degrees-of-freedom
is defined with a vector of displacements $\mathbf{x} = (x_1, \dots, x_j, \dots, x_N)$, where x_j
(Fig. 1) denotes the j -th spatial degree-of-freedom. When base excitation

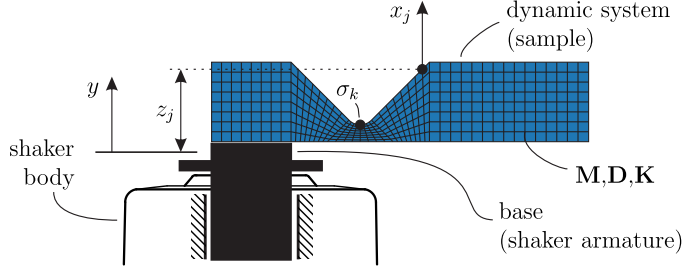


Figure 1: Concept of vibration-fatigue test (to improve clarity, the sample is oversized).

105 is applied to the system in terms of the displacement y the vector of relative displacements between the system and base is $\mathbf{z} = \mathbf{x} - \mathbf{b}y$, where \mathbf{b} is the directional vector between y and \mathbf{x} . Assuming hysteretic damping, the equation of motion for a dynamic system under base excitation is defined as [28]:

$$\mathbf{M} \ddot{\mathbf{z}} + \mathbf{iD} \dot{\mathbf{z}} + \mathbf{K} \mathbf{z} = -\mathbf{M} \mathbf{b} \ddot{y}, \quad (1)$$

110 where the mass matrix \mathbf{M} , damping matrix \mathbf{D} and stiffness matrix \mathbf{K} characterize the system's spatial properties. Solving the left-hand part of Eq. (1) as an eigenvalue problem we can obtain a set of N natural frequencies ω_r and the modal matrix Φ , composed of N mass-normalized mode shapes ϕ_r [24]. The boundary conditions within the latter step must define a zero displacement for the degree-of-freedom at which the base excitation y is applied.
 115 Accordingly, when the excitation (*i. e.*, the right-hand side of Eq. (1)) is taken into account, the response of the sample in terms of relative displacements is defined as [28]:

$$\mathbf{z}(\omega) = \sum_{r=1}^N \frac{\phi_r^T \mathbf{M} \mathbf{b} \ddot{y}(\omega) \phi_r}{\omega_r^2 - \omega^2 + \mathbf{i} \eta_r \omega_r^2}, \quad (2)$$

120 where ϕ_r^T is the excitability and ϕ_r is the responsiveness of the r -th mode shape. Introducing the vector of mode participation factors Γ as [31]:

$$\Gamma = \Phi^T \mathbf{M} \mathbf{b}, \quad (3)$$

the response at the j -th degree-of-freedom in terms of relative displacement (Eq. (2)) can be simplified to:

$$z_j(\omega) = \sum_{r=1}^N \frac{\Gamma_r \phi_{r,j}}{\omega_r^2 - \omega^2 + \mathbf{i} \eta_r \omega_r^2} \cdot \ddot{y}(\omega). \quad (4)$$

When the system's response is sought in terms of the stress vector $\boldsymbol{\sigma}(\omega)$, rather than the relative displacement vector $\mathbf{z}(\omega)$, the responsiveness of the displacement mode shape $\boldsymbol{\phi}_r$ in Eq. (2) is replaced by the stress mode shape $\boldsymbol{\sigma}\boldsymbol{\phi}_r$. The stress response $\sigma_k(\omega)$ at the k -th stress degree-of-freedom (Fig. 1) for excitation with the base excitation can be obtained as:

$$\sigma_k(\omega) = \sum_{r=1}^N \frac{\Gamma_r \boldsymbol{\sigma}\boldsymbol{\phi}_{r,k}}{\omega_r^2 - \omega^2 + i\eta_r \omega_r^2} \cdot \ddot{y}(\omega) = H_{\sigma\ddot{y},k}(\omega) \cdot \ddot{y}(\omega), \quad (5)$$

where $H_{\sigma\ddot{y},k}(\omega)$ is the system's transmissibility from the base kinematics $\ddot{y}(\omega)$ to the stress response $\sigma_k(\omega)$.

When the dynamic system is kinematically excited with a random signal having a known one-sided power spectral density (PSD) $G_{\ddot{y}\ddot{y}}(\omega)$ [32], the response at the k -th stress degree-of-freedom can also be obtained in terms of PSD as $G_{\sigma\sigma,k}(\omega)$ [24]:

$$G_{\sigma\sigma,k}(\omega) = |H_{\sigma\ddot{y},k}(\omega)|^2 G_{\ddot{y}\ddot{y}}(\omega). \quad (6)$$

As summarized in the following Sec. 2.2, $G_{\sigma\sigma,k}(\omega)$ and the material fatigue parameters provide sufficient information to obtain a fatigue-life estimate of the observed dynamic system at the location of the k -th stress degree-of-freedom when spectral-damage-counting methods are used. Obviously, the PSD of the stress response $G_{\sigma\sigma,k}(\omega)$ can be obtained by knowing the PSD of the fundamental acceleration $G_{\ddot{y}\ddot{y}}(\omega)$, and the stress transmissibility $H_{\sigma\ddot{y},k}(\omega)$. $G_{\ddot{y}\ddot{y}}(\omega)$ is usually defined in the control unit of the shaker and maintained by a feedback loop with the control accelerometer. $H_{\sigma\ddot{y},k}(\omega)$ depends on the modal parameters of the system ω_r , η_r , $\boldsymbol{\sigma}\boldsymbol{\phi}_{r,k}$ and Γ_r , which can be obtained from an experiment or a valid digital twin.

2.2. Spectral methods for damage estimation

For a fatigue-life estimation of a mechanical component under a known stress load in the fatigue zone, two assumptions are generally adopted [33]. First is a logarithmic relation between the number of cycles until failure N and the stress cycle amplitude σ , also known as Basquin's law $\sigma = S_f N^b$, where S_f and b present material's properties of fatigue strength and fatigue exponent, respectively. Second, the linear damage accumulation is assumed to be $D = \sum_i n_i/N$, where n_i is the number of cycles at the stress-load amplitude and D denotes the total accumulated damage. When the stress load at the fatigue zone is stationary and available in frequency-, rather than

in the time-domain, we are encouraged to use spectral methods to estimate
 155 the fatigue life [24] to avoid long stress histories and reduce the computational
 effort.

When the component is excited with a random signal in the frequency
 range of a single natural frequency, the stress response can be regarded as a
 narrow-band signal. In such a case the amplitudes of the load-cycles follow a
 160 Rayleigh distribution [34], yielding an analytically deductible relation for the
 damage intensity (*i. e.*, damage over time unit), known as the Narrowband
 method [34]:

$$d^{\text{NB}} = \frac{(\sqrt{2} m_0)^k}{2 \pi C} \sqrt{\frac{m_2}{m_0}} \Gamma\left(1 + \frac{k}{2}\right), \quad (7)$$

where k and C are the alternative notations for material's fatigue properties
 ($k = -1/b$, $C = S_f^{-1/b}$). Γ is the Gamma function and m_0 , m_2 are the
 165 moments of the one-sided stress-response PSD, and are defined as [32]:

$$m_i = \int_0^{+\infty} \omega^i G_{\sigma\sigma}(\omega) d\omega. \quad (8)$$

If the stress time-history in any way deviates from the narrow-band sig-
 nal (broadband signal, bi-modal response, . . .), alternative spectral methods
 should be used [30]. For such cases, the Dirlik method [35] is widely used,
 where the damage intensity is obtained with the equation:

$$d^{\text{DK}} = C^{-1} \nu_p m_0^{k/2} \left[G_1 Q^k \Gamma(1 + k) + \left(\sqrt{2}\right)^k \Gamma(1 + k/2) \left(G_2 |R|^k + G_3 \right) \right], \quad (9)$$

170 where ν_p , Q , R , G_1 , G_2 , G_3 are constants that can be calculated from the spec-
 tral moments m_i , where $i = 0, \dots, 4$. A range of different spectral methods
 exists besides the aforementioned Narrowband and Dirlik methods; the most
 commonly used are available in the open-source package [36].

3. Methodology of accelerated fatigue testing with random excita- 175 tion

For establishing a novel methodology for the fatigue testing of 3D-printed
 samples, which is based on the sample's dynamic stress response under a
 vibration load, first the appropriate geometry of the sample was designed

(Sec. 3.1), followed by the experimental setup (Sec. 3.2) and a valid stress
 180 PSD reconstruction from a digital twin and the measured dynamic response
 of the sample (Sec. 3.3).

3.1. Sample design

The general requirements for the proposed test sample are: manufacturability by FFF (or possibly other 3D-printing technologies), a single critical
 185 fatigue zone on the sample when excited in a specific, well-separated mode shape [37], a uniaxial stress state in the fatigue zone, and repeatability of the boundary conditions when excited with an electrodynamic shaker. Due to the directional printing, the sample geometry must also allow different printing directions in the fatigue zone to observe the anisotropy of the sample's fatigue
 190 properties. In addition, the sample design should allow observation of the fatigue phenomenon over a wide frequency range to investigate the influence of strain rate and loading frequency on the fatigue properties of the sample. The fatigue-testing methodology must be scalable and allow for a reduction in the overall testing time when testing multiple samples simultaneously.

The proposed sample geometry is presented in Fig. 2 and consists of three sections: the section with the fixation surfaces, the thinned section with the fatigue zone and the inertial-mass section for frequency tuning.
 195 The sample is fixed by clamping the marked surfaces with a M8 bolt. By varying the dimension L the sample's first natural frequency can be changed. The sample's first mode shape is presented in Fig. 3.
 200

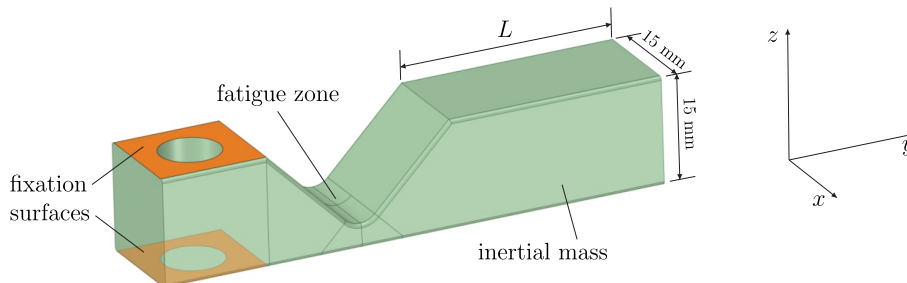


Figure 2: Proposed sample geometry with the reference coordinate system.

In previous studies [12, 27] planar FFF samples were used to observe the influence of the infill raster angle. To reduce the influence of print-layer orientation and the perimeter filaments in [12, 27], the angle between the

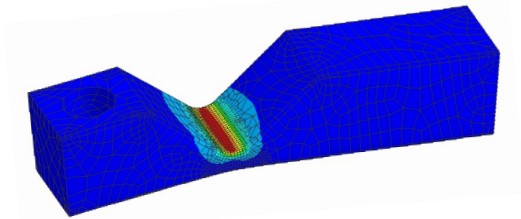


Figure 3: Normal stress distribution in y direction for sample's first mode-shape.

print-layers and the loading direction was kept at 90° and the perimeter filaments did not vary between the samples. However, crack initiation rarely occurs in the interior of the sample, which is characterized by the configuration of infill filaments, and more commonly occurs on the surface of the sample, which is defined by the configuration of the perimeter filaments. Therefore, in this research the sample is sliced in three spatial directions (x , y and z , as noted in Figs. 2 and 4). With that, we can obtain samples with an identical geometry, but different orientations of the perimeter filaments and print-layers compared to the direction of maximum stress load σ_y , see Fig. 4. In this way, it is possible to evaluate the influence of perimeter configuration on the sample's fatigue life. To reduce its influence on fatigue life, in this study the infill was set to a rectilinear pattern with 100% infill density. Further details regarding the tested samples are given in Sec. 4.2.

3.2. Simultaneous fatigue testing of multiple samples with broadband excitation

The proposed test methodology is based on vibration testing with a random vibration signal using an electrodynamic shaker. The underlying concept for determining the fatigue parameters from vibration testing is summarized in Fig. 5 and is presented next. First, the vibration load is defined within the shaker controller in terms of the acceleration PSD $G_{\ddot{y}\ddot{y}}(\omega)$ (6) and controlled by a feedback loop. To reduce the changes in the stress response PSD $G_{\sigma\sigma,k}(\omega)$ due to changes in the sample's natural frequency during the test, the $G_{\ddot{y}\ddot{y}}(\omega)$ was defined with a constant amplitude over the entire excitation-frequency range. The excitation-frequency range includes the first natural frequencies of the tested samples, which vary from sample to sample depending on the length of the inertial mass L . With a wide frequency range of random signal excitation and different weight lengths L between

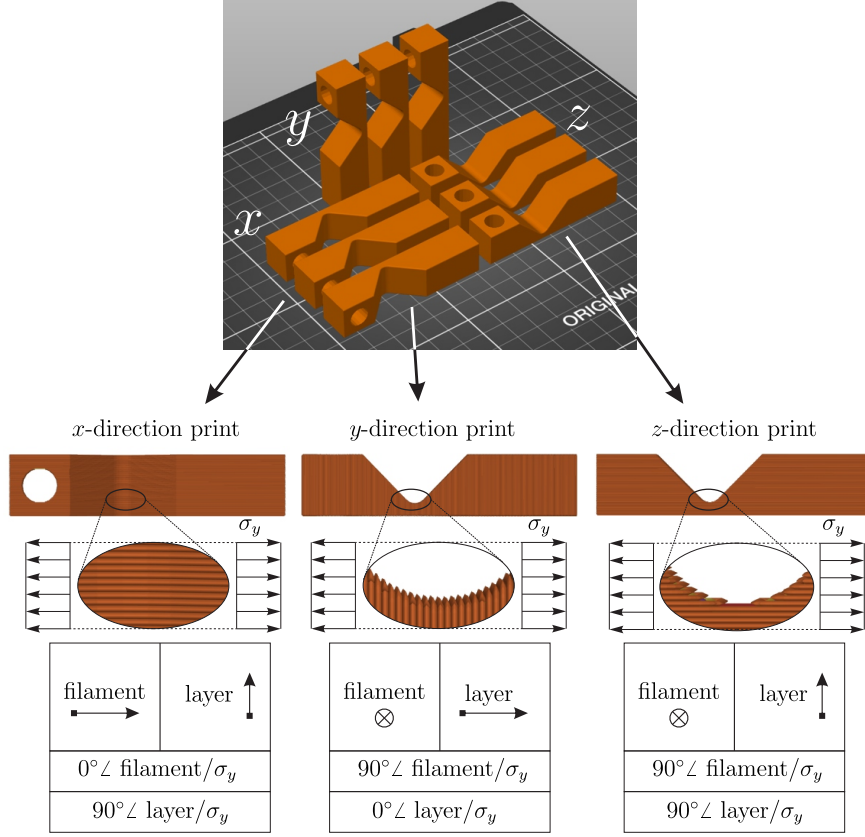


Figure 4: Proposed printing directions and their influence on filament orientation in the sample's fatigue zone.

samples, it is possible to achieve different loading frequencies in a single test and observe their influence on the fatigue parameters.

235 The dynamic response of the sample results in a narrow-band stress in the fatigue zone (Fig. 3), leading to damage accumulation and eventual fatigue failure. Monitoring the actual $G_{\sigma\sigma,k}(\omega)$ on each sample with strain gages would increase the preparation time for the test and could also prove infeasible due to the relatively large strains of the sample's polymer material. Therefore, the response of the sample is monitored with a non-contact laser vibrometer to which a scanning mirror head is attached to monitor multiple
240 samples during testing. In this way the response of the sample is measured in terms of velocity $\dot{x}_j(t)$ (Fig. 5) and, by knowing the excitation signal $\ddot{y}(t)$, the transmissibility $H_{\dot{x}\ddot{y},j}(\omega)$ can be obtained [29]. Applying modal identification

methods [29] we can determine the initial values of the first natural frequency ω_1 and damping ratio η_1 of the sample and their changes during the fatigue test. Combining ω_1 and η_1 with a parametric digital twin (explained in detail in Sec. 3.3), we obtain the valid stress transmissibility $H_{\sigma\ddot{y},k}(\omega)$ (5) and the stress PSD $G_{\sigma\sigma,k}$ (6). Finally, the fatigue parameters b and S_f can be assessed by minimizing the difference between the experimentally determined fatigue life and the calculated fatigue-life estimate using the selected spectral method, see Sec. 2.2.

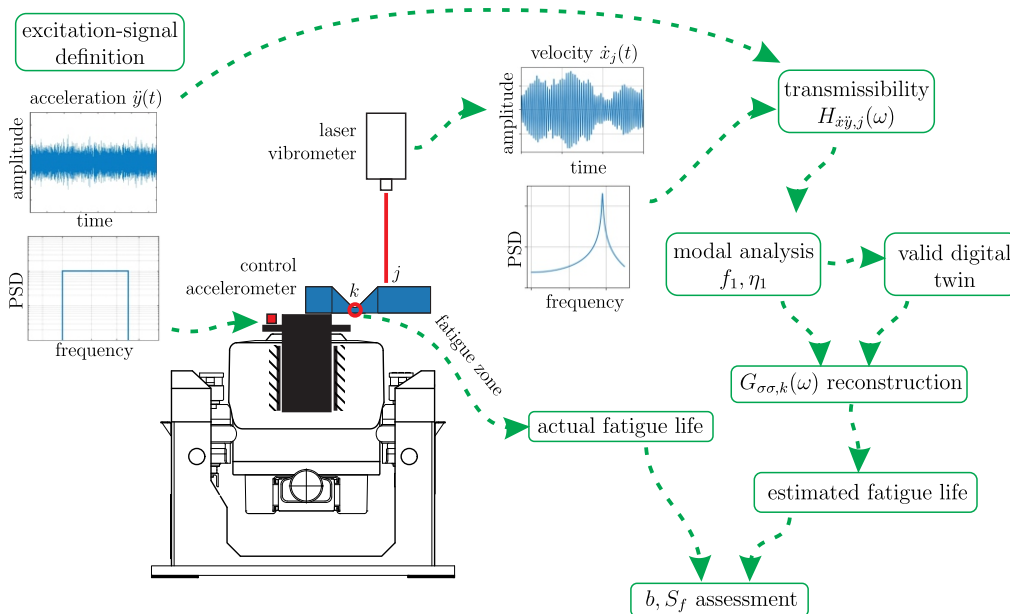


Figure 5: Schematic presentation of testing procedure.

3.3. Digital twin and stress PSD reconstruction

Based on the measurements of transmissibility $H_{\dot{x}\ddot{y},j}(\omega)$, a parametric digital twin is required to obtain a valid reconstruction of the stress PSD $G_{\sigma\sigma,k}(\omega)$ for the fatigue zone. In this research the digital twin was built with input parameters of length L and Young's modulus E . The process of combining the digital twin with measured $H_{\dot{x}\ddot{y},j}(\omega)$ is summarized in Fig. 6 and explained next.

Although the geometry of the sample is well defined, the processing parameters of the FFF and the deviation of the printing material inherently

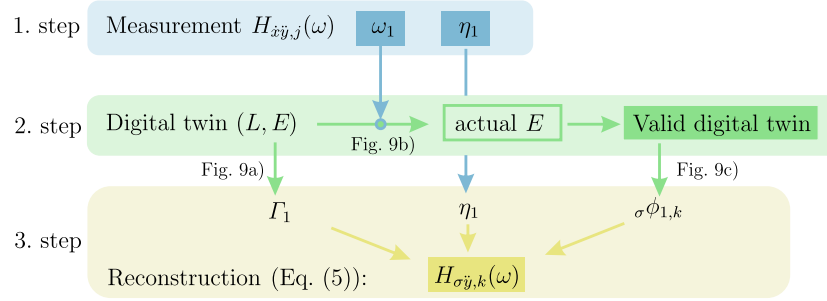


Figure 6: Procedure for $H_{\sigma\ddot{y},k}(\omega)$ reconstruction by combining response measurement and digital twin.

260 lead to differences between the initial digital twin and the sample. Hence, the measurement of $H_{\dot{x}\ddot{y},j}(\omega)$ on the sample and the measured ω_1 and η_1 are used to determine the actual modulus of elasticity E and its damping properties. Once E is known, the digital twin produces a valid first stress mode-shape $\sigma\phi_1$. To obtain the stress transmissibility $H_{\sigma\ddot{y},k}(\omega)$ for the k -th stress degree-
 265 of-freedom in the frequency area of the first natural frequency, only the mode participation factor Γ_1 is still needed (5), which can be numerically obtained from \mathbf{b} , \mathbf{M} and Φ (3) and depends on the sample's geometry (length L) and the material's density ρ , only.

4. Experimental research

270 The proposed method is here tested against 4 different types of samples, manufactured from PLA by FFF. The samples differed in the printing direction as a variation of the processing parameters (x , y or z direction, Fig. 4) and in color as a material variation (blue or gray colorant). This section presents the detailed experimental setup, the processing parameters of each
 275 sample set, the preliminary measurements and the results obtained directly from the fatigue tests.

4.1. Experimental setup

The experimental setup with 8 simultaneously tested samples is shown in Fig. 7. The laser vibrometer Polytec PDV-100 with an attached scanning
 280 head monitored the response of each tested sample. As illustrated in Fig. 7b) for the actual test the j -th degree-of-freedom at the location of the response measurement is denoted with 1 and the k -th stress degree-of-freedom at the

fatigue zone is denoted with 2. The samples were sequentially monitored for 10 seconds to assure good averaging (1 second intervals with 50% overlap and applied Hamming window) of the frequency-response function. The excitation acceleration was measured with a control accelerometer at the fixation adapter. The measurement protocol provided the sample's $H_{\dot{x}\dot{y},1}(\omega)$ every 80 seconds. Such an experimental setup was used for all the samples tested in this study; however, the established methodology can be expanded to a much larger number of simultaneously tested samples.

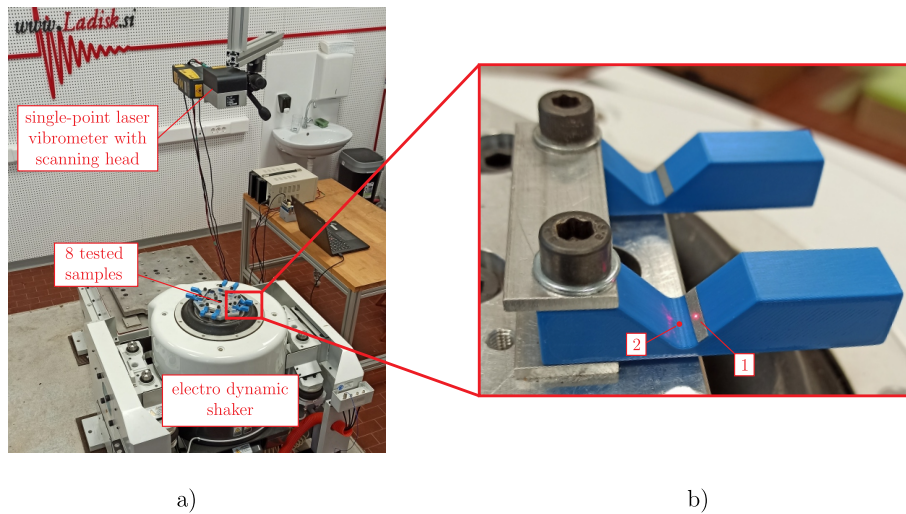


Figure 7: Experimental setup of fatigue test; a) complete setup, b) two tested samples.

4.2. Sample sets, vibration loads and preliminary tests

The samples (Fig. 2) were produced from blue or gray 1.75-mm PLA filaments from the same material supplier (Plastika Trček). For transition from the sample's CAD model to the manufacturable G-code the following settings were used: 0.2-mm layer height, 100% rectilinear infill with 45° raster angle to the global coordinate system (Fig. 2) and 2 layers of perimeter.

The samples were fabricated using a commercially available Prusa i3 MK3S+ 3D printer with the processing parameters as follows: 0.4-mm nozzle diameter, 220°C nozzle temperature, 25 mm/s for external-perimeter printing speed, 45 mm/s for internal-perimeter printing speed and 80 mm/s for infill printing speed. Total production time for a single sample with 30-mm

length L of the inertial mass (Fig. 2) was 65 min and 120 min for z direction and y direction print, respectively.

In addition to the variations in the printing direction and colorant, the weight length L of the samples was also varied between 9 mm and 30 mm in 3-mm increments. The weight length is not directly related to the fatigue properties of the material; however, the length L alters the natural frequency of the sample and therefore can be used to evaluate the effect of the loading frequency on the fatigue parameters of the polymer filament in potential future research. In the present study, 106 samples were tested, distributed over the combinations of influencing parameters given in Tab. 1.

Table 1: Quantity of tested samples.

Fabrication parameter		Weight length L [mm]								
Print direction	Color	30	27	24	21	18	15	12	9	Σ
x	blue	2	2	6	6	0	0	0	0	16
y		4	3	4	3	4	4	4	4	30
z	gray	8	8	8	8	0	0	0	0	32
		0	0	0	0	8	8	6	6	28
$\Sigma\Sigma$										106

The $G_{\dot{y}\dot{y}}(\omega)$ frequency range was set to 200-800 Hz and the levels of $G_{\dot{y}\dot{y}}(\omega)$ were 0.05, 0.1, 0.15, 0.2 and 0.4 g^2/Hz . As the fatigue tests were conducted, eventually the initiation and the progression of the crack appeared on every sample, which resulted in a decrease of its natural frequency, which served as a real-time monitoring of the damage accumulated for an individual sample [37].

In the existing studies on the fatigue of polymeric materials [12, 13, 38], the loading frequencies of classical quasi-static fatigue tests are set to less than 20 Hz, mainly to prevent a significant temperature rise on the sample. Since the samples in this study were loaded at frequencies above 250 Hz, it was necessary to experimentally determine the potential temperature rise on the sample before performing the actual fatigue tests. Hence, the temperature measurements were performed on four pre-samples with maximum weight length L (30 mm) to ensure the maximum value of $\Gamma_1 \cdot \sigma\phi_{1,2}$, *i. e.*, the numerator in $H_{\sigma\dot{y},2}(\omega)$, Eq. (5). The four pre-samples enclosed all the combinations of the processing parameters, stated in Tab. 1, and were tested simultaneously with an acceleration load of $G_{\dot{y}\dot{y}}(\omega)$ level of 0.2 g^2/Hz .

330 With such a combination of sample geometry and vibration load the highest damage rates and lowest fatigue lives were targeted, according to the planned subsequent fatigue tests. The temperatures at the fatigue zones of the pre-samples and the temperature on the fixation plate were measured with a Telops FAST M3k infrared camera. The measured temperatures are presented in Fig. 8, from which we can observe the maximum increase of the temperature is 5°C. With the glass-transition temperature of the 3D-printed PLA being 55-65°C [39] it was concluded that the temperature rise to 27°C 335 (i. e., 4°C above ambient temperature) is acceptable.

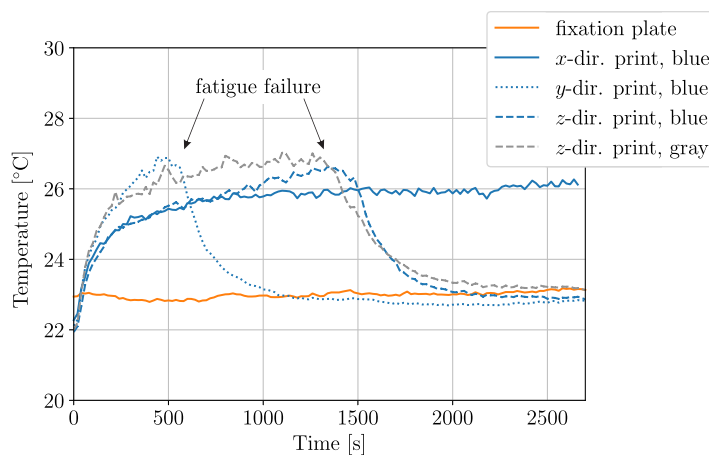


Figure 8: Temperature on pre-samples during fatigue test.

4.3. Reconstruction of $G_{\sigma\sigma,2}(\omega)$

340 Following the procedure for reconstruction of $H_{\sigma\dot{y},2}(\omega)$ (Eq. 4, Fig. 6), the parametric digital twin and the measurement of $H_{\dot{x}\dot{y},1}(\omega)$ are required. The output variables of the parametric digital twin are summarized in Fig. 9. The samples are excited at the first natural frequency and therefore the location of the fatigue failure is identical for all the samples. Consequently, a single mode participation factor Γ_1 and a single stress modal constant for the critical stress degree-of-freedom $\sigma\phi_{1,2}$ are needed from the digital twin, Figs. 9a) and 9c), 345 respectively. Further, the damping ratio η_1 is obtained from the measurement (Fig. 6) and with known pre-defined level of excitation PSD $G_{\dot{y}\dot{y}}(\omega)$ the stress PSD $G_{\sigma\sigma,2}(\omega)$ (6) can be fully reconstructed. The transition from measured $H_{\dot{x}\dot{y}}(\omega)$ to a valid reconstruction of $G_{\sigma\sigma,2}(\omega)$ (6) is shown in Fig. 10 on an

350 actual sample with label SN001 and weight length $L = 21$ mm. It should be emphasized that with the presented approach a valid reconstruction of $G_{\sigma\sigma,2}(\omega)$ can be performed on-the-fly for every tested sample without any computational effort.

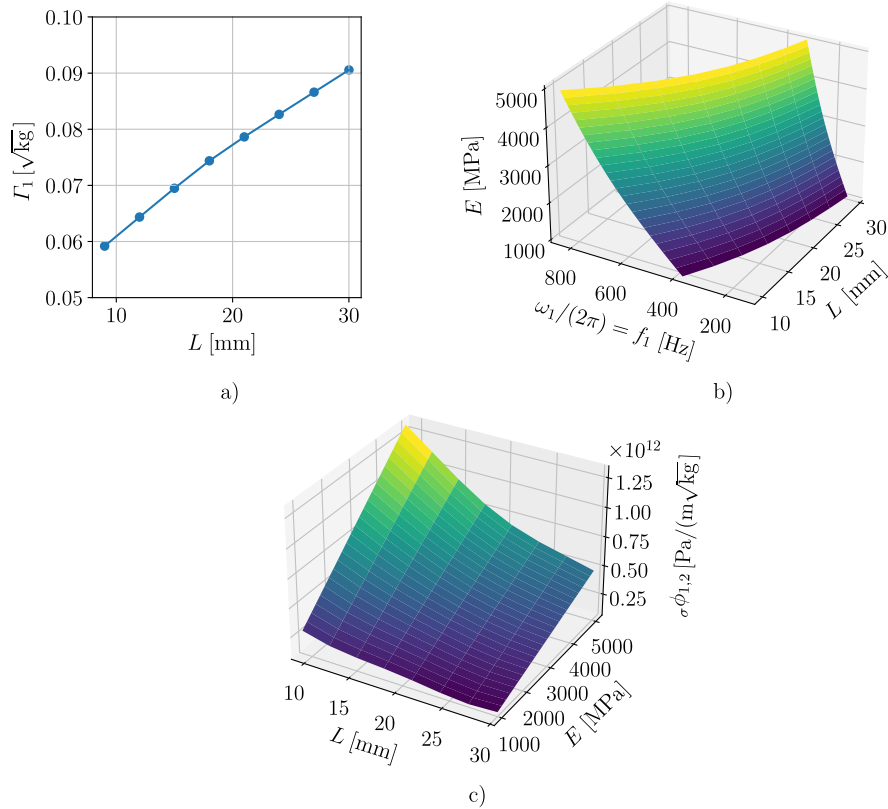


Figure 9: Parametric model results, required for valid reconstruction of $G_{\sigma\sigma,2}(\omega)$ for given weight length L and measured natural frequency f_1 ; a) mode-participation factor for first mode shape $\Gamma_1(L)$, b) Young's modulus $E(L, f_1)$, c) stress modal constant $\sigma\phi_{1,2}(L, E)$ at the fatigue zone.

4.4. Experimental results

355 By monitoring an individual sample's FRF the observations of modal parameters at the beginning and throughout the test were possible before the actual assessment of the material's fatigue parameters and are presented next. The measured $H_{\hat{x}\hat{y},1}(\omega)$ were evaluated with the Least-Squares Com-

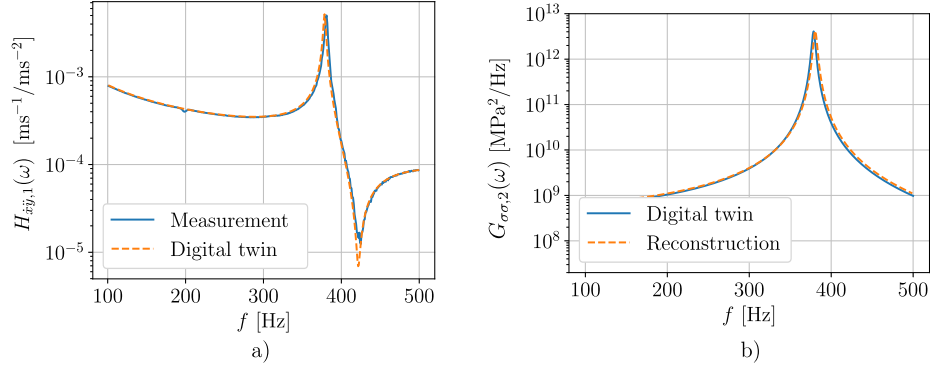


Figure 10: Dynamic properties of sample SN001, a) measured and modeled transmissibility $H_{\hat{x}ij,1}(\omega)$, b) modeled and reconstructed $G_{\sigma\sigma,2}(\omega)$ for $G_{\hat{y}y}(\omega)$ with constant level of $0.1 \text{ g}^2/\text{Hz}$.

plex Frequency (LSCF) algorithm implemented in an open-source Python
 360 package pyEMA [40] by setting the highest order of the polynomial to 10.

Fig. 11 presents the initial values of the samples's natural frequencies from
 which we can observe good repeatability between samples with equal fabri-
 cation parameters and a low influence of the printing direction. However, a
 significant difference is observed for the natural frequencies between samples
 365 with different colors, although the material and geometry should be identi-
 cal for samples with the same weight length. Further, Fig. 12 and Tab. 2
 present the initial damping ratios of the undamaged tested samples. There,
 we can observe significantly higher mean values of the damping ratios for the
 samples made from gray filament. Additionally, observing the blue samples,
 370 the samples printed in the y direction show higher standard deviations when
 compared to the samples printed in the x and z directions.

Both modal parameters, the natural frequency and damping ratio, which
 have a direct influence on the $G_{\sigma\sigma,2}(\omega)$ at the fatigue zone, are evidently sub-
 jected to significant uncertainties and hence cannot be estimated beforehand
 375 without any experimental activities either for the estimation of the expected
 fatigue life or for an assessment of the fatigue parameters for particular fab-
 rication conditions.

Fig. 13 shows the changes of the natural frequencies for all the tested sam-
 ples during the fatigue test, grouped by fabrication parameters. Evidently,
 380 the samples within a particular sample set show good repeatability concern-
 ing the frequency-drop rate once the natural frequency begins to decrease.

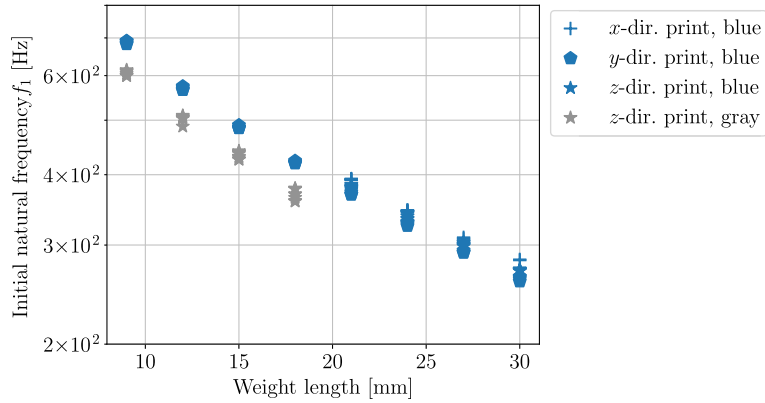


Figure 11: Natural frequencies of samples before the fatigue test.

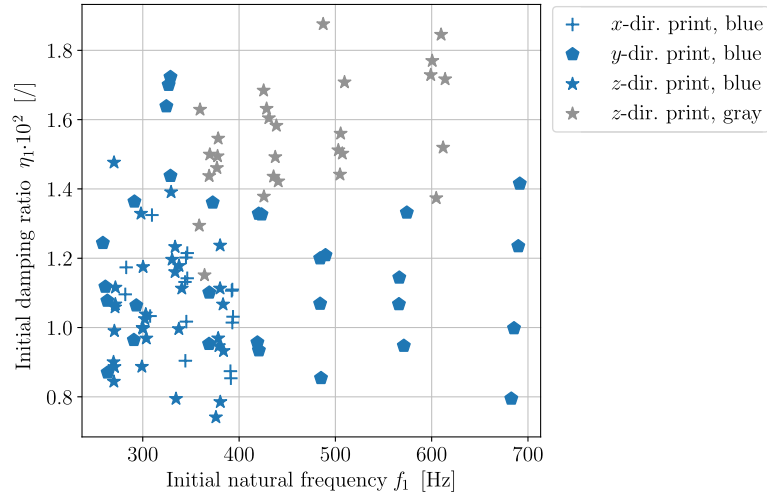


Figure 12: Damping ratios of undamaged tested samples.

385 On the other hand, the distinct differences regarding the frequency-drop rate are manifested between the four sample sets and indicate the significant influence of the print direction and also, to a certain extent, the influence of the colorant. Fig. 14 presents the development of damping ratios for the tested samples during the fatigue tests. In addition to the information about the initial damping values (Fig. 12), we can observe that the damping ratios increase according to the natural-frequency drop and are strongly dependent on the crack propagation.

Table 2: Initial damping ratios η_1 of sample sets.

Print direction	Color	Damping ratio $\eta_1 \cdot 10^2$	
		Mean	St. dev.
x	blue	1.08	0.12
y		1.18	0.24
z		1.05	0.17
	gray	1.55	0.16

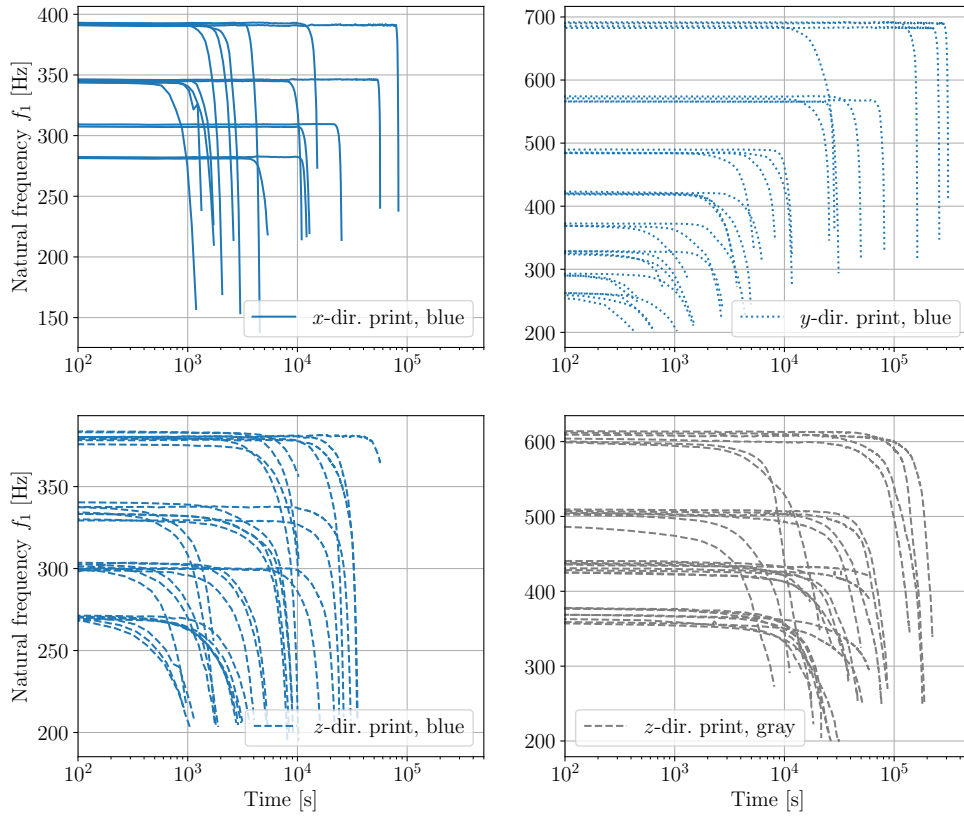


Figure 13: Decrease of natural frequency f_1 for tested samples.

390 5. Results and discussion

In vibration fatigue, significant changes in natural frequencies and damping ratios are regularly observed before complete breakage of the test-sample occurs. For metal structures, a threshold of a 2.5% frequency drop is com-

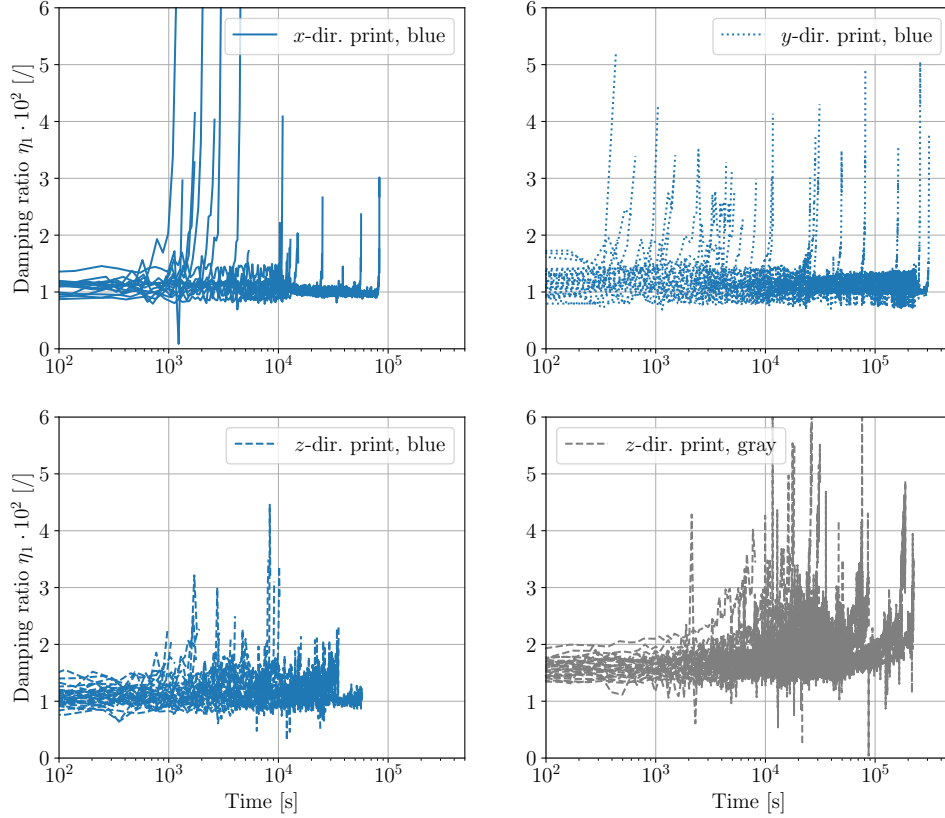


Figure 14: Increase of damping ratio η_1 for tested samples.

monly adopted for declaring the fatigue failure of a tested sample [41, 42].
 395 For 3D-printed PLA samples, the natural-frequency drop can occur in the
 earlier stages of fatigue test (Fig. 13); therefore, the reference drop in this
 study is increased to 5%. It should be noted that the $G_{\sigma\sigma,2}(\omega)$ of an individ-
 ual sample was reconstructed using the average value of the damping ratio
 η_1 during the identified fatigue life.

400 Fig. 15a) shows the number of load cycles until the frequency drop thresh-
 old is reached for different stress loads, characterized by the estimation vari-
 able σ_{RMS} ; the results resemble the linear trend on a logarithmic scale ob-
 tained by the classical quasi-static fatigue test, and confirm the applicability
 of the proposed approach for fatigue testing. Evidently, a large number of
 405 load cycles can be achieved in a relatively short time; for example, sample

SN107 marked in Fig. 15a) with $f_1=690$ Hz reached $2.08 \cdot 10^8$ load cycles in 83.6 hours. However, due to the random signal excitation, the load amplitude is variable and corresponds to the Rayleigh distribution, as shown for sample SN107 in Fig. 15b). From this, it can be seen that the endurance limit of $2 \cdot 10^6$ cycles was exceeded for amplitude ranges below 5.5 MPa.

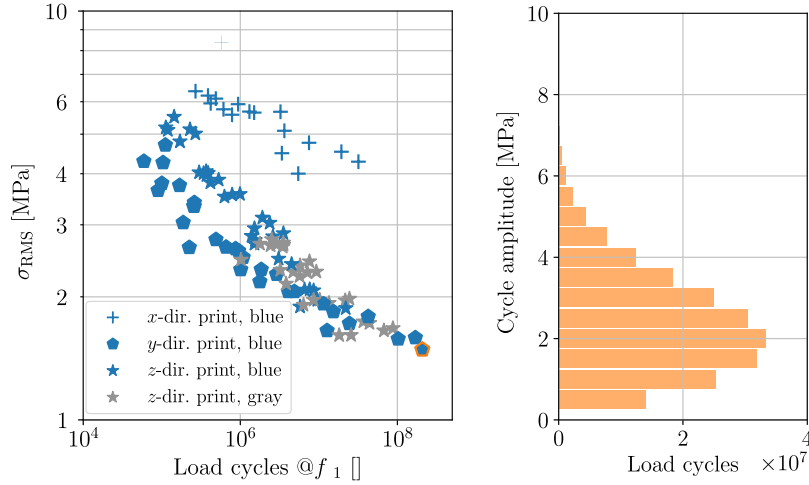


Figure 15: a) Fatigue lives, presented in load cycles at first natural frequency f_1 until failure at σ_{RMS} , b) cycle amplitude distribution for sample SN107.

5.1. Assessment of fatigue parameters

σ_{RMS} and the number of load cycles at the first natural frequency f_1 are not a direct measure of damage rate in the fatigue zone; therefore, the material fatigue parameters b and S_f cannot be extracted from the results shown in Fig. 15a). To obtain an accurate damage rate and, consequently, to assess the fatigue parameters of a particular sample type, the appropriate spectral method (Sec. 2.2) should be applied to the reconstructed $G_{\sigma\sigma,2}(\omega)$. In the present research, the Dirlik method (Eq. (9)) was applied, providing a fast and reliable estimate of the damage rate, even in cases with increased damping or bimodal response, which could be investigated with the proposed methodology in future studies.

Based on the linear characteristic of the SN curve on a logarithmic scale, a cost function $Q(b, S_f)$ between the actual and estimated fatigue lives for

425 a particular set of N samples was defined as the variance of the differences
between T_{act} and T_{est} :

$$Q(b, S_f) = \frac{1}{N} \sum_{i=1}^N (\log_{10}(T_{\text{act},i}) - \log_{10}(T_{\text{est},i}(b, S_f)))^2. \quad (10)$$

Evaluation of $Q(b, S_f)$ for a particular sample set within the expected
ranges of b and S_f provides a single global minimum where the amount of
the experimental results (Fig. 15) improves the localization of the optimal
430 (b, S_f) pair.

Fig. 16 shows the assessed fatigue parameters along with the comparison
between the actual and estimated fatigue lives for observed sample sets and
95% confidence intervals. From Fig. 16 a good correlation is evident for both
sample sets printed in the z direction, while sample sets printed in the x
435 and y directions show wider confidence intervals. For the samples printed
in the x direction, the larger deviations from the predicted mean occur at
longer fatigue lives and lower load values. The set of samples printed in
the y direction, unlike the remaining three sample sets, covers a complete
range of weight lengths (Tab. 1) and consequent load frequencies (Fig. 11);
440 its deviation from the predicted mean in Fig. 16 indicates the possibility of
frequency-dependent fatigue parameters for PLA. With the established test-
ing methodology, the phenomenon of frequency-dependent fatigue param-
eters can be effectively investigated and represents one of the short-term chal-
lenges. However, the obtained results are valid for loading frequency ranges
445 generally observed in environmental testing and do not represent an extrap-
olation of fatigue results at lower operating frequencies of fatigue-testing
machines.

The obtained SN curves for particular sample sets are presented in Fig. 17
together with the relevant results from the literature. Focusing first on the re-
450 sults obtained with novel accelerated-fatigue-testing methodology, it is clear
that the printing direction and consequently the orientation of the perimeter
filaments have a large impact on the durability of the 3D-printed structures.
Comparing the expected number of cycles for identical PLA material at a
load amplitude of 10 MPa, the fatigue life of the sample can be prolonged
455 from $1.4 \cdot 10^4$ cycles for samples printed in the y direction, to $8.3 \cdot 10^4$ cycles
for samples printed in the z direction, to $7.0 \cdot 10^6$ cycles for samples printed
in the x direction. To put this in a different perspective: by changing the
manufacturing direction of 3D-printed PLA structures, we can improve the

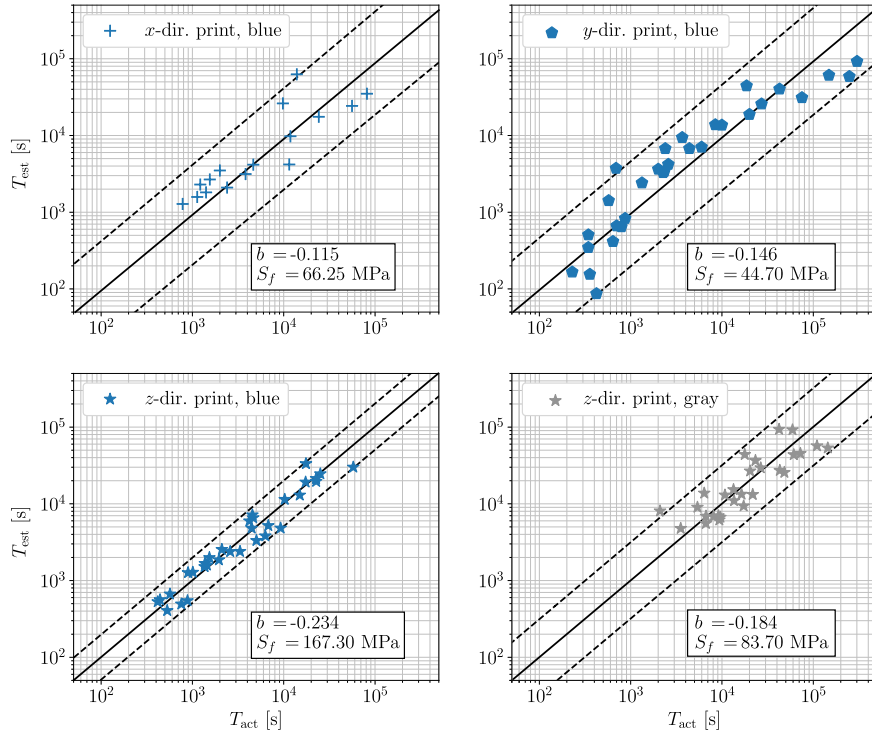


Figure 16: Comparison of actual and estimated fatigue lives for assessed fatigue parameters for tested sample sets with marked 95% confidence intervals.

durability of the structure by a factor of 500, well over two orders of mag-
460 nitude. Here, it should be noted that, as expected, the samples printed
in the x and y directions represent the most fatigue-resistant and the least
fatigue-resistant sample types, respectively (Fig. 4). As confirmed by the ex-
perimental results, the highest fatigue life of the 3D-printed PLA structure
465 can be achieved when the perimeter filaments are parallel to the principal
stress, while maintaining the same processing parameters. In order to achieve
optimal fatigue life of the PLA mechanical components under high-cycle fati-
gure, parallelism between the layer normal and the principal stress should
be avoided at all locations where stresses exceed 40% of the maximum load
stress on the component.

470 Further examination shows a very good agreement between PLA samples
with different colorant, printed in the z direction. Such good correlation
was not expected beforehand, considering that there are relevant differences
between the Young's modulus of the material [43], evident in the different

values of the natural frequency in Fig. 13 and also between the damping
475 ratios of the samples (Fig. 12 and Tab. 2), where the mean values differ
by almost 50%. Another important point that can be derived from these
results is the importance of including the actual damping ratios in the fatigue-
life evaluation. Slight changes in sample damping can lead to a significant
change in the stress-response PSD which result in discrepancies of fatigue-life
480 estimates [44]. The exact damping ratio for the individual sample tested is
provided by the established methodology and is also included in the fatigue-
parameter assessment, increasing the reliability of the results obtained and
the subsequent fatigue-life estimates.

Only slight differences can be observed between the samples printed in the
485 y and z directions, especially in the area of high-cycle fatigue. For low-cycle
fatigue, the samples printed in the z direction exhibit higher fatigue resis-
tance. This is an important observation for mechanical parts designed for
low-cycle fatigue life, when the optimal perimeter filament cannot be assured
on critical locations. In such cases, the layer-normal should be perpendicu-
490 lar to the maximum principal stress to achieve the highest possible fatigue
resistance.

The available fatigue data from previous studies [11, 12, 27] do not give a
unanimous answer about the fatigue properties of PLA. This is not a surprise
because, for example, Vanaei et al. [45] in a single study observed a 10-fold
495 change in the fatigue life of PLA samples just by varying the printing tem-
perature by 10°C. If different PLA manufacturers and variable fatigue test
conditions (especially loading frequency) are taken into account in addition
to different processing parameters, some scatter between the results of differ-
ent studies is to be expected. This is also shown in Fig. 17, which presents
500 a comparison between the SN curves of PLA obtained with the newly in-
troduced vibration-fatigue methodology and previous studies obtained with
classical fatigue tests at lower frequencies [12, 27] or with the rotational
bending fatigue test [11, 46]. In general, the new methodology of accelerated
fatigue testing with random excitation provides similar fatigue resistivity of
505 the material in the case of well-oriented filaments (x direction print) when
compared to a similar sample design in [27] and to the most robust samples
in [12]. Good agreement with existing studies is also evident for the less
favourable orientation of the filament (printed in y and z directions) com-
pared to a similar sample design in [46] and to a rectilinear-infill pattern
510 without perimeter layers in [12]. The obtained SN curves are on the slightly
conservative side also due to the low threshold for the frequency drop of 5%

from the initial value.

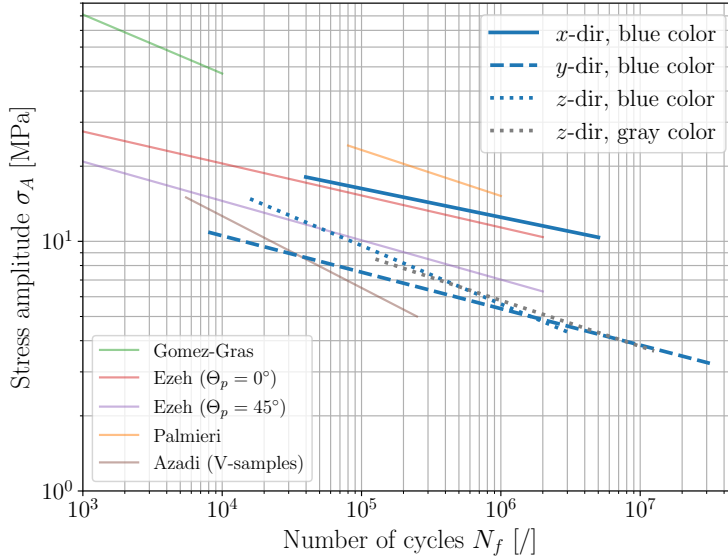


Figure 17: SN curves for the sample sets studied and comparison with previous studies [11, 12, 27, 46].

6. Conclusions

This research work deals with the vibration fatigue of PLA mechanical parts manufactured with FFF. The proposed method of accelerated fatigue testing involves the random signal excitation of FFF samples with innovative geometry design, allowing an evaluation of different manufacturing and environmental parameters in relation to fatigue resistance, with particular attention on the orientation of the perimeter filaments. Although significant uncertainties are inherent to any dynamically excited 3D-printed structure, this study overcomes the problem by constructing a digital twin for an individual sample. Compared to classical fatigue testing, the proposed methodology of accelerated fatigue testing with random excitation offers several enhancements, especially for polymer FFF components:

- Fatigue testing is performed in the frequency range of actual environmental testing, eliminating the uncertainty due to the extrapolation of

test results obtained at lower loading frequencies.

- The proposed method can identify and quantify the frequency-dependent fatigue properties of a material.
- 530 • With minimal effort (sample preparation, indirect stress PSD measurement with a vibrometer) and in significantly less time, meaningful and reliable results can be obtained. In this study, the effective test time for 106 test samples is 226 hours.
- 535 • Shorter testing times allow for a larger number of samples tested in a given time. Consequently, the proposed method is suitable for a comprehensive evaluation of various processing and environmental factors on the fatigue properties of 3D-printed components and could also be used for quality assurance between different PLA batches, if applied appropriately.
- 540 • The novel fatigue-testing methodology simultaneously provides information about the development of the natural frequency and damping ratio during damage accumulation; this information is required for valid numerical modeling and can be also proven relevant for structural health monitoring during service life.

545 In the presented study, special attention was paid to confirm the reliability of the new method of accelerated fatigue testing. The results presented in this manuscript regarding the fatigue parameters of the samples from FFF PLA show a considerable mutual correlation as well as a good agreement with the available data from previous studies. Considering the shorter times
550 for conducting the fatigue test, the newly introduced methodology is best suited to fatigue testing on larger sample sets. In all, the presented method of accelerated fatigue testing with random vibration represents a fast and reliable method of fatigue test that provides an additional information about the fatigue resistance of dynamically loaded 3D-printed components.

555 **References**

- [1] I. Gibson, D. Rosen, B. Stucker, M. Khorasani, Additive Manufacturing Technologies, 2nd Edition, Springer Cham, Baldock, Hertfordshire, 2000.

- 560 [2] T. Košir, J. Slavič, Single-process fused filament fabrication 3D-printed high-sensitivity dynamic piezoelectric sensor, *Additive Manufacturing* 49 (2022) 102482. doi:<https://doi.org/10.1016/j.addma.2021.102482>.
- 565 [3] J. Tan, H. Low, Embedded electrical tracks in 3D printed objects by fused filament fabrication of highly conductive composites, *Additive Manufacturing* 23 (2018) 294–302. doi:<https://doi.org/10.1016/j.addma.2018.06.009>.
- 570 [4] D. Munghen, V. Iacobellis, K. Behdinan, Incorporation of fiber Bragg grating sensors in additive manufactured Acrylonitrile butadiene styrene for strain monitoring during fatigue loading, *International Journal of Fatigue* 154 (2022) 106485. doi:<https://doi.org/10.1016/j.ijfatigue.2021.106485>.
- 575 [5] M. Askari, D. A. Hutchins, P. J. Thomas, L. Astolfi, R. L. Watson, M. Abdi, M. Ricci, S. Laureti, L. Nie, S. Freear, R. Wildman, C. Tuck, M. Clarke, E. Woods, A. T. Clare, Additive manufacturing of metamaterials: A review, *Additive Manufacturing* 36 (2020) 101562. doi:<https://doi.org/10.1016/j.addma.2020.101562>.
- 580 [6] M. R. Khosravani, F. Berto, M. R. Ayatollahi, T. Reinicke, Characterization of 3D-printed PLA parts with different raster orientations and printing speeds, *Scientific Reports* 12 (2022). doi:<https://doi.org/10.1038/s41598-022-05005-4>.
- 585 [7] J. Luo, Q. Luo, G. Zhang, Q. Li, G. Sun, On strain rate and temperature dependent mechanical properties and constitutive models for additively manufactured polylactic acid (PLA) materials, *Thin-Walled Structures* 179 (2022) 109624. doi:<https://doi.org/10.1016/j.tws.2022.109624>.
- 590 [8] S. Rouf, A. Raina, M. Irfan Ul Haq, N. Naveed, S. Jeganmohan, A. Farzana Kichloo, 3D printed parts and mechanical properties: Influencing parameters, sustainability aspects, global market scenario, challenges and applications, *Advanced Industrial and Engineering Polymer Research* 5 (3) (2022) 143–158. doi:<https://doi.org/10.1016/j.aiepr.2022.02.001>.

- 595 [9] M. F. Afrose, S. H. Masood, P. Iovenitti, M. Nikzad, I. Sbarski, Effects of part build orientations on fatigue behaviour of FDM-processed PLA material, *Progress in Additive Manufacturing* 1 (2016) 21–28. doi:
<https://doi.org/10.1007/s40964-015-0002-3>.
- [10] R. Jerez-Mesa, J. Travieso-Rodriguez, J. Llumà-Fuentes, G. Gomez-Gras, D. Puig, Fatigue lifespan study of PLA parts obtained by additive manufacturing, *Procedia Manufacturing* 13 (2017) 872–879. doi:
<https://doi.org/10.1016/j.promfg.2017.09.146>.
- 600 [11] G. Gomez-Gras, R. Jerez-Mesa, J. A. Travieso-Rodriguez, J. Lluma-Fuentes, Fatigue performance of fused filament fabrication PLA specimens, *Materials & Design* 140 (2018) 278–285. doi:
<https://doi.org/10.1016/j.matdes.2017.11.072>.
- [12] O. Ezeh, L. Susmel, Fatigue strength of additively manufactured polylactide (PLA): effect of raster angle and non-zero mean stresses, *International Journal of Fatigue* 126 (2019) 319–326. doi:
605 <https://doi.org/10.1016/j.ijfatigue.2019.05.014>.
- [13] O. Ezeh, L. Susmel, On the notch fatigue strength of additively manufactured polylactide (PLA), *International Journal of Fatigue* 136 (2020) 105583. doi:
610 <https://doi.org/10.1016/j.ijfatigue.2020.105583>.
- [14] J. Mayén, A. Del Carmen Gallegos-Melgar, I. Pereyra, C. A. Poblano-Salas, M. Hernández-Hernández, J. Betancourt-Cantera, V. Mercado-Lemus, M. Del Angel Monroy, Descriptive and inferential study of hardness, fatigue life, and crack propagation on PLA 3D-printed parts, *Materials Today Communications* 32 (2022) 103948. doi:
615 <https://doi.org/10.1016/j.mtcomm.2022.103948>.
- [15] F. He, M. Khan, Effects of printing parameters on the fatigue behaviour of 3D-printed ABS under dynamic thermo-mechanical loads, *Polymers* 13 (14) (2021). doi:
<https://doi.org/10.3390/polym13142362>.
- 620 [16] C. Ziemian, R. Ziemian, Residual strength of additive manufactured ABS parts subjected to fatigue loading, *International Journal of Fatigue* 134 (2020) 105455. doi:
<https://doi.org/10.1016/j.ijfatigue.2019.105455>.

- 625 [17] J. A. Travieso-Rodriguez, M. D. Zandi, R. Jerez-Mesa, J. Lluma-Fuentes, Fatigue behavior of PLA-wood composite manufactured by fused filament fabrication, *Journal of Materials Research and Technology* 9 (4) (2020) 8507–8516. doi:<https://doi.org/10.1016/j.jmrt.2020.06.003>.
- 630 [18] S. Terekhina, T. Tarasova, S. Egorov, I. Skornyakov, L. Guillaumat, M. Hattali, The effect of build orientation on both flexural quasi-static and fatigue behaviours of filament deposited PA6 polymer, *International Journal of Fatigue* 140 (2020) 105825. doi:<https://doi.org/10.1016/j.ijfatigue.2020.105825>.
- 635 [19] X. Li, J. He, Z. Hu, X. Ye, S. Wang, Y. Zhao, B. Wang, Y. Ou, J. Zhang, High strength carbon-fiber reinforced polyamide 6 composites additively manufactured by screw-based extrusion, *Composites Science and Technology* 229 (2022) 109707. doi:<https://doi.org/10.1016/j.compscitech.2022.109707>.
- 640 [20] J. Zhang, V. Hirschberg, D. Rodrigue, Mechanical fatigue of biodegradable polymers: A study on polylactic acid (PLA), polybutylene succinate (PBS) and polybutylene adipate terephthalate (PBAT), *International Journal of Fatigue* 159 (2022) 106798. doi:<https://doi.org/10.1016/j.ijfatigue.2022.106798>.
- 645 [21] M. S. A. Parast, A. Bagheri, A. Kami, M. Azadi, V. Asghari, Bending fatigue behavior of fused filament fabrication 3D-printed ABS and PLA joints with rotary friction welding, *Progress in Additive Manufacturing* (2022). doi:<https://doi.org/10.1007/s40964-022-00307-5>.
- 650 [22] V. Shanmugam, O. Das, K. Babu, U. Marimuthu, A. Veerasimman, D. J. Johnson, R. E. Neisiany, M. S. Hedenqvist, S. Ramakrishna, F. Berto, Fatigue behaviour of FDM-3D printed polymers, polymeric composites and architected cellular materials, *International Journal of Fatigue* 143 (2021) 106007. doi:<https://doi.org/10.1016/j.ijfatigue.2020.106007>.
- 655 [23] R. J. Crawford, P. J. Martin, *Plastics Engineering*, 4th Edition, Butterworth-Heinemann, 2020.
- [24] J. Slavič, M. Mršnik, M. Česnik, J. Javh, M. Boltežar, *Vibration Fatigue by Spectral Methods*, 1st Edition, Elsevier, 2020.

- [25] F. Xue, G. Robin, H. Boudaoud, F. A. Cruz Sanchez, E. M. Daya, General methodology to investigate the effect of process parameters on the vibration properties of structures produced by additive manufacturing using fused filament fabrication, *JOM* 74 (3) (2022). doi:<https://doi.org/10.1007/s11837-021-05051-9>.
660
- [26] F. Medel, J. Abad, V. Esteban, Stiffness and damping behavior of 3D printed specimens, *Polymer Testing* 109 (2022) 107529. doi:<https://doi.org/10.1016/j.polymertesting.2022.107529>.
665
- [27] M. Palmieri, G. Zucca, G. Morettini, L. Landi, F. Cianetti, Vibration fatigue of FDM 3D printed structures: The use of frequency domain approach, *Materials* 15 (3) (2022). doi:[10.3390/ma15030854](https://doi.org/10.3390/ma15030854).
- [28] D. J. Ewins, *Modal Testing: Theory, Practice and Application*, 2nd Edition, Research Studies Press Ltd., Baldock, Hertfordshire, 2000.
670
- [29] N. M. M. Maia, J. M. M. Silva, *Theoretical and Experimental Modal Analysis*, Research Studies Press Ltd., Baldock, Hertfordshire, 1997.
- [30] M. Mršnik, J. Slavič, M. Boltežar, Frequency-domain methods for a vibration-fatigue-life estimation – Application to real data, *International Journal of Fatigue* 47 (2013) 8–17. doi:<https://doi.org/10.1016/j.ijfatigue.2012.07.005>.
675
- [31] H. Seon Park, J. Kim, B. K. Oh, Model updating method for damage detection of building structures under ambient excitation using modal participation ratio, *Measurement* 133 (2019) 251–261. doi:<https://doi.org/10.1016/j.measurement.2018.10.023>.
680
- [32] J. S. Bendat, A. G. Piersol, *Random Data: Analysis and Measurement Procedures*, 4th Edition, Wiley, 2010.
- [33] Y.-L. Lee, J. Pan, R. B. Hathaway, M. E. Barkey, *Fatigue Testing and Analysis; Theory and Practice*, 1st Edition, Elsevier, Oxford, 2005.
- [34] J. W. Miles, On structural fatigue under random loading, *Journal of the Aeronautical Sciences* 21 (11) (1954) 753–762. doi:[10.2514/8.3199](https://doi.org/10.2514/8.3199).
685
- [35] T. Dirlik, *Application of computers in fatigue analysis*, Ph.D. thesis, University of Warwick (1985).

- 690 [36] A. Zorman, J. Slavič, Flife, <https://github.com/ladisk/FLife> (2022).
- [37] M. Česnik, J. Slavič, M. Boltežar, Uninterrupted and accelerated vibrational fatigue testing with simultaneous monitoring of the natural frequency and damping, *Journal of Sound and Vibration* 331 (24) (2012) 5370–5382. doi:<https://doi.org/10.1016/j.jsv.2012.06.022>.
- 695 [38] C. Capela, S. Oliveira, J. Ferreira, Fatigue behavior of short carbon fiber reinforced epoxy composites, *Composites Part B: Engineering* 164 (2019) 191–197. doi:<https://doi.org/10.1016/j.compositesb.2018.11.035>.
- [39] A. A. B. A. Bakar, M. Z. B. Zainuddin, A. N. B. Adam, I. S. B. M. Noor, N. B. Tamchek, M. S. B. Alauddin, M. I. B. M. Ghazali, The study of mechanical properties of poly(lactic) acid PLA-based 3D printed filament under temperature and environmental conditions, *Materials Today: Proceedings* 67 (2022) 652–658. doi:<https://doi.org/10.1016/j.matpr.2022.06.198>.
- 700 [40] K. Zaletelj, T. Bregar, D. Gorjup, J. Slavič, pyema, <https://github.com/ladisk/pyEMA> (2020).
- [41] L. Capponi, M. Česnik, J. Slavič, F. Cianetti, M. Boltežar, Non-stationarity index in vibration fatigue: Theoretical and experimental research, *International Journal of Fatigue* 104 (2017) 221–230. doi:<https://doi.org/10.1016/j.ijfatigue.2017.07.020>.
- 710 [42] M. Mršnik, J. Slavič, M. Boltežar, Multiaxial vibration fatigue—a theoretical and experimental comparison, *Mechanical Systems and Signal Processing* 76-77 (2016) 409–423. doi:<https://doi.org/10.1016/j.ymsp.2016.02.012>.
- 715 [43] B. Wittbrodt, J. M. Pearce, The effects of PLA color on material properties of 3-D printed components, *Additive Manufacturing* 8 (2015) 110–116. doi:<https://doi.org/10.1016/j.addma.2015.09.006>.
- [44] M. Česnik, J. Slavič, Vibrational fatigue and structural dynamics for harmonic and random loads, *Journal of Mechanical Engineering* 60 (5) 720 (2014) 339–348. doi:<https://10.5545/sv-jme.2013.1831>.

- 725 [45] H. Vanaei, M. Shirinbayan, S. Vanaei, J. Fitoussi, S. Khelladi, A. Tcharkhtchi, Multi-scale damage analysis and fatigue behavior of PLA manufactured by fused deposition modeling (FDM), Rapid Prototyping Journal 27 (2) (2020) 371–378. doi:10.1108/RPJ-11-2019-0300.
- 730 [46] M. Azadi, A. Dadashi, S. Dezianian, M. Kianifar, S. Torkaman, M. Chiyani, High-cycle bending fatigue properties of additive-manufactured ABS and PLA polymers fabricated by fused deposition modeling 3D-printing, Forces in Mechanics 3 (2021) 100016. doi:https://doi.org/10.1016/j.finmec.2021.100016.